and the neck extended perpendicular to the bond axis through large-scale atomic motion. For PbSe NCs, considerable atomic reconfigurations have been reported (*13*, *14*). The necking explains the elongation of the bond lengths, which also results in a considerably more open honeycomb structure than can be obtained from geometric attachment of rigid block models (Fig. 1H, as compared with the real structures in Figs. 1, A to C, 3, and 4). In the mechanism that we propose, not all of the capping molecules have to be released at once from a facet, resulting in pathways with lower activation energy. Oriented attachment accompanied with neck formation has been reported before as a pathway for the growth of various metal nanoparticles (*15*, *16*).

Since the emergence of graphene (*17*), there has been a general interest in the properties of electrons confined in a honeycomb lattice (*18*–*23*). We show that oriented attachment can form the basis of a generally applicable two-step method for the preparation of 2D semiconductors with nanoscale honeycomb geometry: assembly and oriented attachment of Pb-chalcogenide NCs with truncated cubic shape, followed by cation exchange. It has been predicted that honeycomb semiconductors of zinc blende compounds (such as CdSe) show a truly new electronic band structure, with a valence hole Dirac band and one or two conduction electron Dirac bands combined with strong spin-orbit coupling (*6*). We transformed PbSe honeycomb structures into CdSe superlattices via a cation exchange reaction (*24*, *25*) and showed that honeycomb structures can also be prepared from PbS NCs (figs. S12 and S13).

The successful exchange of a PbSe honeycomb lattice into a CdSe honeycomb is presented in Fig. 4. The complete transformation of the PbSe lattice into CdSe is confirmed by means of energy-dispersive x-ray spectroscopy (fig. S14). HAADF-STEM and ED measurements show that the orientation of the Se anion lattice with respect to the honeycomb periodicity is preserved (Fig. 4, A to C). This result is in agreement with earlier described mechanisms in which the anion lattice is preserved during cation exchange (*26*, *27*) and is corroborated with high-resolution HAADF-STEM measurements of honeycomb structures at intermediate stages of cation exchange (*7*).

REFERENCES AND NOTES

1. C. Pacholski, A. Kornowski, H. Weller, *Angew. Chem. Int. Ed. Engl.* **41**, 1188–1191 (2002).
2. K.-S. Cho, D. V. Talapin, W. Gaschler, C. B. Murray, *J. Am. Chem. Soc.* **127**, 7140–7147 (2005).
3. W. K. Koh, A. C. Bartnik, F. W. Wise, C. B. Murray, *J. Am. Chem. Soc.* **132**, 3909–3913 (2010).
4. C. Schliehe *et al.*, *Science* **329**, 550–553 (2010).
5. W. H. Evers *et al.*, *Nano Lett.* **13**, 2317–2323 (2013).
6. E. Kalesaki *et al.*, *Phys. Rev. X* **4**, 011010 (2014).
7. Materials and methods are available as supplementary materials on *Science* Online.
8. H. Friedrich *et al.*, *Nano Lett.* **9**, 2719–2724 (2009).
9. M. P. Boneschanscher *et al.*, *Nano Lett.* **13**, 1312–1316 (2013).
10. P. A. Midgley, M. Weyland, *Ultramicroscopy* **96**, 413–431 (2003).
11. The PbSe honeycombs suffer from beam damage, making it hard to obtain high-quality tomographic reconstructions. CdSe, on the other hand, is more stable under the electron beam, resulting in higher-quality tomographic reconstructions (Fig. 3 as compared with fig. S9, for example. Both images are obtained under the same conditions).
12. D. Li *et al.*, *Science* **336**, 1014–1018 (2012).
13. M. A. van Huis *et al.*, *Nano Lett.* **8**, 3959–3963 (2008).
14. M. A. van Huis *et al.*, *Adv. Mater.* **21**, 4992–4995 (2009).
15. J. M. Yuk *et al.*, *Science* **336**, 61–64 (2012).
16. J. M. Yuk *et al.*, *Chem. Commun. (Camb.)* **49**, 11479–11481 (2013).
17. A. H. Castro Neto, N. M. R. Peres, K. S. Novoselov, A. K. Geim, *Rev. Mod. Phys.* **81**, 109–162 (2009).
18. K. K. Gomes, W. Mar, W. Ko, F. Guinea, H. C. Manoharan, *Nature* **483**, 306–310 (2012).
19. G. De Simoni *et al.*, *Appl. Phys. Lett.* **97**, 132113 (2010).
20. M. Gibertini *et al.*, *Phys. Rev. B* **79**, 241406 (2009).
21. C.-H. Park, S. G. Louie, *Nano Lett.* **9**, 1793–1797 (2009).
22. C.-H. Park, L. Yang, Y.-W. Son, M. L. Cohen, S. G. Louie, *Phys. Rev. Lett.* **101**, 126804 (2008).
23. A. Singha *et al.*, *Science* **332**, 1176–1179 (2011).
24. J. M. Luther, H. Zheng, B. Sadtler, A. P. Alivisatos, *J. Am. Chem. Soc.* **131**, 16851–16857 (2009).
25. B. J. Beberwyck, Y. Surendranath, A. P. Alivisatos, *J. Phys. Chem. C* **117**, 19759–19770 (2013).
26. S. Bals *et al.*, *Nano Lett.* **11**, 3420–3424 (2011).
27. M. Casavola *et al.*, *Chem. Mater.* **24**, 294–302 (2012).

ACKNOWLEDGMENTS

We thank ESRF (Grenoble, France) for providing the synchrotron beamtime and the staff of ESRF beamline ID-01 for their support. We thank C. van Overbeek for his help on the PbS sample. This research is part of the programs "Control over Functional Nanoparticle Solids (FNS)" and "Designing Dirac Carriers in semiconductor honeycomb superlattices (DDC)," which are supported by the Foundation of Fundamental Research on Matter (FOM), which is part of the Dutch Research Council (NWO). The authors also acknowledge financial support from the European Research Council (ERC Advanced Grant 24691-COUNTATOMS and ERC Starting Grant #335078-COLOURATOM). The authors also appreciate financial support from the European Union under the Seventh Framework Program [Integrated Infrastructure Initiative 262348 European Soft Matter Infrastructure (ESMI)]. This work was supported by the Flemish Fund for Scientific Research (FWO Vlaanderen) through a Ph.D. research grant to B.G.

SUPPLEMENTARY MATERIALS

www.sciencemag.org/content/344/6190/1377/suppl/DC1
Materials and Methods
Figs. S1 to S14
Tables S1 to S2
References (*28*, *29*)
Movies S1 to S2

25 February 2014; accepted 13 May 2014
Published online 29 May 2014;
10.1126/science.1252642

NANOMATERIALS

Hydroxylation of the surface of PbS nanocrystals passivated with oleic acid

Danylo Zherebetskyy,[1] Marcus Scheele,[1,2] Yingjie Zhang,[1,3] Noah Bronstein,[2] Christopher Thompson,[1,2] David Britt,[4] Miquel Salmeron,[1] Paul Alivisatos,[1,2] Lin-Wang Wang[1]*

Controlling the structure of colloidal nanocrystals (NCs) is key to the generation of their complex functionality. This requires an understanding of the NC surface at the atomic level. The structure of colloidal PbS NCs passivated with oleic acid has been studied theoretically and experimentally. We show the existence of surface OH^- groups, which play a key role in stabilizing the PbS(111) facets, consistent with x-ray photoelectron spectroscopy as well as other spectroscopic and chemical experiments. The role of water in the synthesis process is also revealed. Our model, along with existing observations of NC surface termination and passivation by ligands, helps to explain and predict the properties of NCs and their assemblies.

The structure of the interior of nanocrystals (NCs) can be determined quite accurately by crystallography, but the structure of their surfaces cannot be obtained from this analysis because of the complexity of the organic capping ligands (*1*–*6*). However, the NC surface structure controls the growth and solubility and strongly influences the physical and chemical properties (*7*–*12*). We took advantage of improved insights into the mechanisms of NC growth (*3*–*6*), combined with extensive ab initio total energy calculations, to create a testable model for the atomic surface passivation structure of the exposed facets of a PbS NC. The model made specific, and at first surprising, predictions about the surface-bound species that were subsequently verified experimentally. PbS is ideal for this study because of the high symmetry of its rock-salt structure and its propensity to form NCs with well-defined (111) and (001) facets (*13*, *14*). PbS NCs with controlled size and shape can be produced from a PbO lead precursor, hexamethyldisilathiane (TMS_2S) sulfur precursor, and oleic acid that binds to exposed Pb atoms to stabilize the surface (*1*–*6*).

We performed ab initio electronic structure calculations on relevant subsystems and on the reaction steps involved in the synthetic process, including studies of immediate precursors, the fate of byproducts of the initial decomposition step, NC-ligand interactions, and ligand-ligand and ligand-solvent

[1]Materials Sciences Division, Lawrence Berkeley National Laboratory, Berkeley, CA 94720, USA. [2]Department of Chemistry, University of California at Berkeley, Berkeley, CA 94720, USA. [3]Applied Science and Technology Graduate Program, University of California at Berkeley, Berkeley, CA 94720, USA. [4]The Molecular Foundry, Lawrence Berkeley National Laboratory, One Cyclotron Road, Berkeley, CA 94720, USA.
***Corresponding author. E-mail: lwwang@lbl.gov**

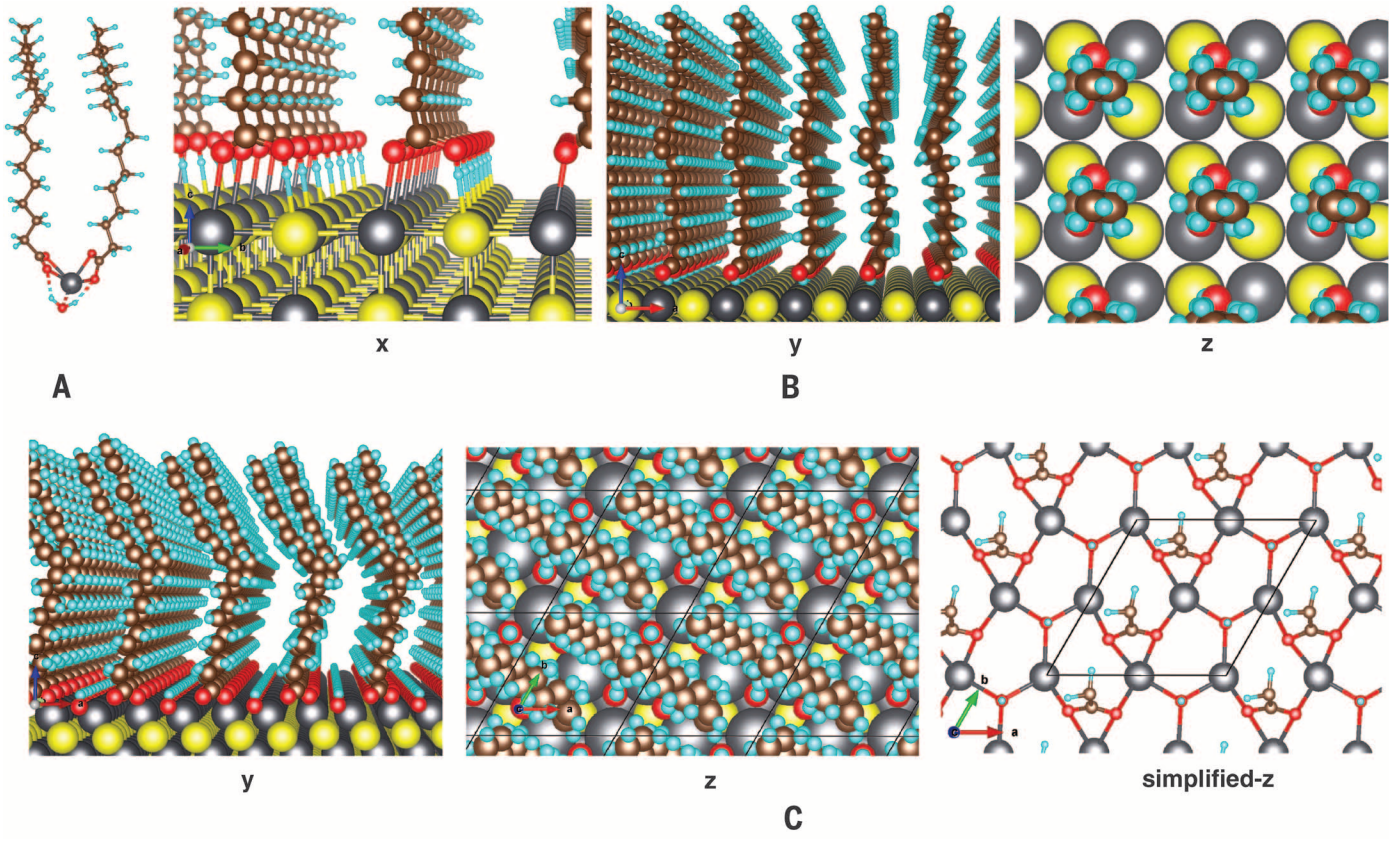

Fig. 1. Optimized molecular configurations. (**A**) A water molecule formed during NC synthesis is bound to the $Pb(OA)_2$ molecule, forming a $Pb(OA)_2\cdots H_2O$ complex. (**B**) Relaxed configuration of OAH molecules on the PbS(001) surface (*x*,*y*,*z* views). (**C**) Relaxed lowest-energy configuration of OA^- and OH^- molecules on the PbS(111) surface: *y* and *z* views. On the right, a simplified *z*-view schematic is shown with truncated tail chains. Pb, gray; S, yellow; O, red; H, blue; C, brown.

interactions. Our methods (*15*) are density functional theory (DFT) in the generalized gradient approximation (GGA). The GGA is not accurate enough to describe the van der Waals (vdW) interactions, and the entropic contributions in the solvent are prohibitively time-consuming at present to be calculated directly. However, we have taken advantage of likely cancellations of these terms when comparing different systems. We found the following features in our theoretically derived model: (i) The Pb:S atomic ratio is roughly 1.2:1 (Pb_{excess}:S ~ 0.2:1) for ~5-nm NCs. (ii) The ratio between the number of surface oleate molecules and the number of excess Pb atoms is ~1:1. (iii) The ligands can be easily removed from the (001) surface. (iv) The average (111)/(001) surface-to-center distance ratio of the truncated octahedral shape is about 0.82:1. (v) OH^- groups are present on the NC (111) facet. These features are consistent with prior and current experimental studies, including Rutherford backscattering (RBS), transmission electron microscopy (TEM), x-ray photoelectron spectroscopy (XPS), sum frequency generation (SFG) spectroscopy, nuclear magnetic resonance (NMR), and Fourier transform infrared spectroscopy (FTIR) (*5*, *6*, *16*–*18*). The presence of hydroxide groups on the surface predicted in the calculation as by-products of precursor decomposition was verified with XPS and SFG. The existence of water in the precursor was supported with NMR and FTIR measurements.

Table 1. Surface and ligand binding energies for the (001) and (111) surfaces of a PbS NC. The (001) and (111) surface areas per OAH (OA^-) molecule are 35.2 and 30.5 $Å^2$, respectively.

	(001)	(111)
Unpassivated surface (meV/$Å^2$)	12.31	23.47*
Binding *E* per OAH (or OA^-) (eV)	−0.16	−0.52
Total surface energy (meV/$Å^2$)	7.76	6.33

*Reconstructed surface.

The colloidal PbS NCs (*4*, *5*) are synthesized by dissolving PbO in hot oleic acid (*15*). One of the by-products of the reaction is water, which was proposed to remain as free molecules in the solution (*4*, *5*). Our calculations, however, show that it is energetically more favorable for water to bind to the Pb precursor (*15*). Thus, the first reaction step can be written as

$$PbO + 2 \times OAH \rightarrow Pb(OA)_2\cdots H_2O \quad (1)$$

where OAH denotes oleic acid. The DFT-optimized structure of the $Pb(OA)_2\cdots H_2O$ is shown in Fig. 1A. In the experiment, the reaction products were degassed at 110°C under vacuum for 1 hour. To determine whether such degassing removed all of the water in the precursor as previously suggested, we used NMR and FTIR. Although NMR demonstrated the absence of liquid water, it was unable to distinguish water molecules bound to the $Pb(OA)_2$ complexes (*15*). Using FTIR measurements and deuterated oleic acid (d1-OA), we distinguished O-H stretching modes associated with water bound to $Pb(OA)_2$ (*15*). The d1-OA was prepared so that only the acid H was exchanged for D. A major part of the water remained after degassing in sufficient amounts to provide the required 20% of water in Eq. 1 for the surface passivation described below (Pb_{excess}:S = 0.2:1, one OH^- per excess Pb). The existence of water is consistent with the observation that the $Pb(OA)_2$ precursors often form clusters (*19*). As a further demonstration of the role of water, we added acetic anhydride (*20*) as a drying agent during the reaction of Eq. 1, followed by evacuation to remove acetic acid and excess anhydride (*15*). The subsequent formation of PbS NCs was much slower and the NCs were of reduced size, from 8 to 10 nm (for that particular synthesis condition) to 4 nm. Also, the particle shapes became rather irregular, with many (001) surfaces (*15*), which is consistent with our model.

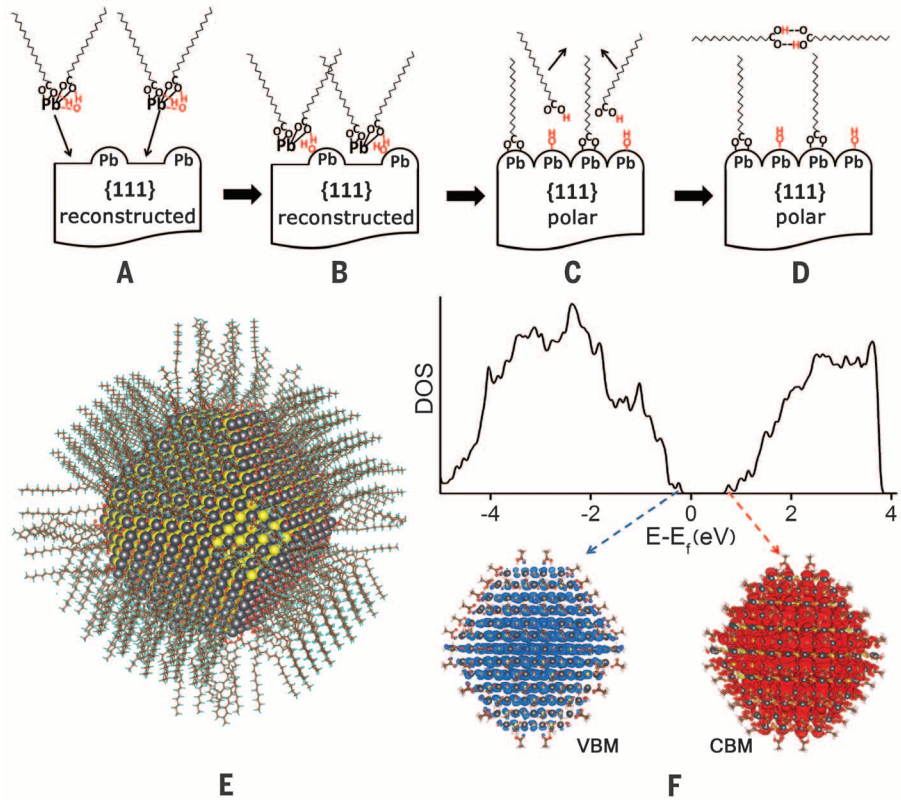

Fig. 2. Model of a PbS NC in colloidal solution. (**A** to **D**) Multistep process for building up the (111) facets of a PbS NC. (A) $Pb(OA)_2\cdots H_2O$ precursors approach the nonpolar and stoichiometric (111) facets. (B) Pb ions bind to surface vacancies. (C) One of the two OA^- in each $Pb(OA)_2\cdots H_2O$ complex is removed because of steric effects, and the water molecule dissociates to provide an OH^- group to the surface and H^+ for desorbing OA^-. (D) The desorbed OAH molecules dimerize in the solvent. (**E**) Calculated atomic structure of a 5-nm-diameter NC passivated with OA^- and OH^- ligands [coordinates in (*15*)]. (**F**) Electron density of states, showing the valence band maximum (VBM) and conduction band minimum (CBM) levels, of a NC passivated with truncated oleic acid alkyl chains [coordinates in (*15*)].

In the second step, TMS_2S dissolved in trioctylphosphine (TOP) is injected into the heated $Pb(OA)_2\cdots H_2O$ precursor dissolved in octadecene

$$Pb(OA)_2\cdots H_2O + (TMS)_2S \rightarrow PbS + (TMS)_2O + 2 \times OAH \quad (2)$$

The calculated Gibbs energy (ΔG) of Eq. 2 is –2.13 eV. It was suggested that the end product from oleic acid is $(oleyl\text{-}CO)_2O$ (*4*, *5*). It is also known, and computationally confirmed, that water will react with $(oleyl\text{-}CO)_2O$ to form two oleic acid molecules. Thus, during NC synthesis, oleic acid, $Pb(OA)_2\cdots H_2O$ [from excess $Pb(OA)_2$ precursor], $(TMS)_2O$, TOP, and octadecene are present in the solution as possible passivants. In the following, we consider passivations of the (001) and (111) surfaces separately.

Our calculation shows that oleic acid has the strongest binding energy to the (001) surface, because of its -COOH group (*15*). The (001) surface covered by OA^- (*9*) has a much higher energy than when covered by OAH, because the OA^- can bind with a cation in the solvent and thus has a much lower chemical potential in the solvent than OAH. On the PbS (001) surface, the -COOH groups form bidentate bridges between Pb and S atoms (–C=O···Pb and -COH···S bonds; Fig. 1B). This model contains one OAH molecule per two surface PbS pairs: one pair bound to one OAH and the other unbound. A high-density packing, with one OAH per PbS pair, is unfavorable because of steric repulsions between the oleyl tails. The binding energy between oleic acid and the PbS (001) surface is calculated as

$$E(\text{bind}) = E(\text{mol/surf}) - [E(\text{mol}) + E(\text{surf})] \quad (3)$$

Here E(mol/surf) is the energy of the whole system, E(surf) is the energy of the unpassivated nonpolar PbS(001) surface after atomic relaxation, and E(mol) is the free energy of the passivating molecule in the solvent, including solvent binding effects. There are two types of solvent binding effects: hydrogen bonding (H bonding) between functional groups and vdW interactions between alkane chains; of these, only H bonding can be described accurately by the GGA method. For the vdW interaction, we have removed the GGA vdW alkyl chain-chain interaction energy from the E(mol/surf) term in Eq. 3, because the chain-chain vdW interactions will approximately cancel each other between the E(mol/surf) term and E(mol) term (*15*). For E(mol), we included the –0.83-eV binding energy of the H-bonded OAH-OAH dimer. We also ignored the entropy change of the ligand molecules, which we deem to be small (*15*). The final calculated (001) binding energy is –0.16 eV per oleic acid (Table 1).

Table 2. Ligand patterns binding energies (in eV) on the (111) PbS NC surface for a 4-Pb-atom area. For $Pb(OA)_2$ cases, the binding energy of H_2O with $Pb(OA)_2$ and the binding of liquid water [after $Pb(OA)_2$ is bound to the surface] are taken into account. The 2 OA^-, 2 OH^- (current model) value is twice that shown in Table 1, because the surface area is twice as large here. The 2 OA^-, O^{2-} corresponds to the case where 2 OH^- form one O^{2-} on the surface and one H_2O leaving the surface.

2 OA^-, 2 OH^-	–1.04
2 OA^-, O^{2-}	–0.60
$Pb(OA)_2$ half-filled	–0.03
$2Pb(OA)_2$ full-filled	+3.78

Assessing the energetics of capping the polar (111) facets is more complicated because of the need for charge compensation (*21*, *22*) to satisfy the electron counting rule (*23*–*25*). The NCs formed in Eq. 2 have equal numbers of Pb and S, with stoichiometric nonpolar (111) facets with only half of the terminal Pb atoms (*22*, *26*). We then considered whether the $Pb(OA)_2\cdots H_2O$ group in the solvent can fill in the surface vacancies (the missing Pb atoms). We found that, in agreement with Bealing *et al.* (*9*), it is sterically impossible to fill every missing Pb atom of the (111) surface with one $Pb(OA)_2$, but one OA^- per missing Pb is possible. Hence, an anionic species is needed for charge balance. This species is OH^-, provided by the dissociation of bound H_2O, while the H^+ is used to form OAH

$$(PbS)_N(111) + Pb(OA)_2\cdots H_2O \rightarrow OA - Pb_{N+1}S_N(111) - OH + OAH \quad (4)$$

Here $(PbS)_N(111)$ denotes the reconstructed nonpolar (111) surface, and $Pb_{N+1}S_N(111)$ denotes the full Pb-terminated polar surface (Fig. 2, A to D). The binding energy of this passivation, which equals to the ΔG of the reaction (*4*), is –0.52 eV per oleate (Table 1), which is much larger than the (001) surface binding energy. The minimum energy configuration (*15*) of OA-$Pb_{N+1}S_N$(111)-OH is shown in Fig. 1C, where the OA^- group stabilizes the Pb ions via μ^2-bidentate bridging bonds, and the OH^- group stabilizes the Pb ions via μ^3-Pb_3–OH bonds. In the calculation of ΔG, we included the OAH-OAH dimer interaction of –0.83 eV and removed the alkyl chain-chain vdW interaction at the surface as in the (001) surface case. Although we have considered other possible passivation stoichiometries and configurations (*15*), none was found to be as stable as the ones considered above (Table 2).

In order to predict the shape of the PbS NC, we calculated the surface energies of the (001) and (111) surfaces, which are equal to the unpassivated surface energies [nonpolar for (111)] plus the binding energies calculated above. The unpassivated

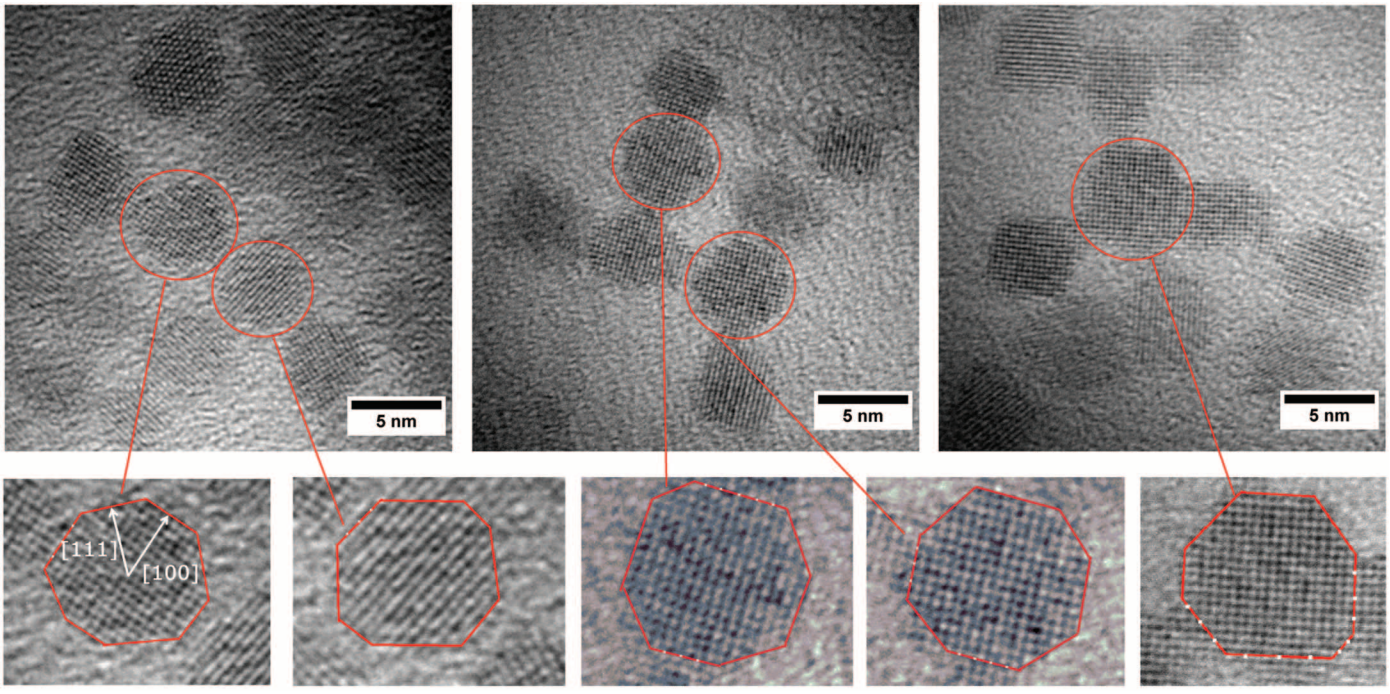

Fig. 3. TEM images of PbS NCs. High-resolution TEM images of the synthesized PbS NCs, with enlarged views of selected NCs shown below. The (111)/(001) Wulff ratios of center-to-surface distances of NCs are 0.820, 0.762, 0.866, 0.847, and 0.792 from left to right, respectively, with an average ratio of 0.817, in good agreement with the calculated value.

Fig. 4. The XPS spectra of PbS NCs. O 1s XPS showing peaks at 531.2eV (red) from O in OH^- groups, and at 532.1eV (green) from O in carboxyl groups. The peak at 534 eV is due to substrate O bound to graphite. a.u., arbitrary units.

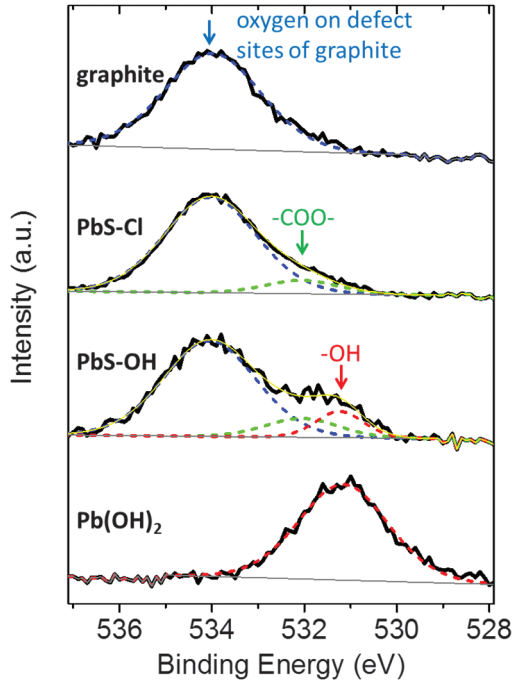

surface energies were calculated from the energies of the slabs minus the corresponding bulk values. The resulting energies (Table 1) were used in a Wulff construction model (*27*–*29*) to determine the equilibrium NC shape. We obtained a (001)-to-(111) Wulff ratio of 0.82, which is in excellent agreement with the average 0.82 value derived from TEM images (Fig. 3). With this procedure, we constructed a model NC with all the surface passivation features (*15*) and with OH^- groups placed at the edges to determine whether it provides good passivation of edges and corners. To simplify the calculation, we truncated the alkyl chains of the oleic acids to the shorter acetic acid, which is not expected to change the NC surface electronic structure. We subsequently relaxed the atomic structure of the 2325-atom, 4–nm-diameter NC using DFT/GGA (*15*). The final system showed perfect surface passivation, with a clean band gap, without impurity or defect-induced states (Fig. 2F) and with good edge and corner passivation. Thus, we propose that the three-dimensional (3D) bulk structure determines the 2D surface passivation structure, which in turn determines the 1D edge passivation. For a 5-nm NC, our model (*15*) also provides the ratio between excess Pb and S atoms of 0.19:1 and between excess Pb and surface OA molecules of 1.18:1 respectively, which agree closely with experimentally observed values of 0.21:1 (measured by RBS) and 0.97:1 reported in (*6*). In our model, the ligand binding energy on the (001) surface is much smaller than that on the (111) surface, consistent with the images in Fig. 3, where all NCs are standing up on (001) facets, with some in direct contact via (001) facets. Both observations indicate that it is easy to remove the ligand molecules from the (001) facets.

One of the most interesting features of our passivation model is the existence of the OH^- groups on the (111) facet. Water readily dissociates into OH^- and H^+ on transition-metal or oxide surfaces (*30*–*33*), and the binding of H_2O to $Pb(OA)_2$ in the solvent provides a natural kinetic pathway for this reaction (Fig. 2, A to D). The presence of small-sized anions is also required to establish charge neutrality over the entire quantum dot that could not be achieved by the sterically hindered OA^- molecules alone. The coexistence of sterically demanding ligands such as OA^-, and small anions to fill the gaps and fulfill the electron counting rule, could apply to other metal chalcogenide systems as well.

To probe the existence of OH^-, two NC samples were synthesized, one as described above (denoted PbS-OH) and another following the procedure developed by Moreels *et al.* (*17*) that uses Cl^- and no water during synthesis [denoted PbS-Cl (*15*)]. In the PbS-Cl sample, the Cl^- anion has effectively replaced OH^-. Both samples were spin-coated on freshly cleaved graphite, followed by thorough washing with acetone to remove unbound ligands, to form a submonolayer film. The XPS data, including those for the two control samples, graphite and $Pb(OH)_2$ powder, are shown in Fig. 4. Although the graphite is freshly cleaved in an Ar glove box (with an oxygen concentration of less than 1 part per million), it is slightly oxidized (*34*, *35*), showing an O 1s peak at 534.0 eV. Because of the incomplete surface coverage (*15*), this substrate peak is also present in the PbS-Cl and PbS-OH NC samples. After subtracting this peak, the PbS-Cl shows only one additional peak at 532.1 eV, probably from the oleate species. The PbS-OH sample contains three peaks at 534.0, 532.1, and 531.2 eV. The new peak at 531.2 eV is assigned to OH^-, in agreement with the $Pb(OH)_2$ powder single peak at 531.2 eV and with reported values for other metal-OH groups' XPS peaks (*36*, *37*). In the PbS-Cl sample, this feature is absent, whereas the Cl species produced a peak in the XPS (*15*). The 534.0-eV and 532.1-eV peaks have the same widths in different samples in Fig. 4. The SFG measurement also indicates the existence of OH^- in the sample (*15*). Although the present work applies to PbS-NCs, we expect the general applicability of this approach to other colloidal NCs.

REFERENCES AND NOTES

1. P. Alivisatos, *Science* **271**, 933–937 (1996).
2. B. Murray *et al.*, *IBM J. Res. Dev.* **45**, 47–56 (2001).
3. Y. Yin, A. P. Alivisatos, *Nature* **437**, 664–670 (2005).
4. J. S. Steckel, B. K. Yen, D. C. Oertel, M. G. Bawendi, *J. Am. Chem. Soc.* **128**, 13032–13033 (2006).
5. H. Liu, J. S. Owen, A. P. Alivisatos, *J. Am. Chem. Soc.* **129**, 305–312 (2007).
6. I. Moreels, B. Fritzinger, J. C. Martins, Z. Hens, *J. Am. Chem. Soc.* **130**, 15081–15086 (2008).
7. J. Li, L. W. Wang, *Nano Lett.* **3**, 1357–1363 (2003).
8. J. Schrier, L. W. Wang, *J. Phys. Chem. C* **112**, 11158–11161 (2008).
9. C. R. Bealing, W. J. Baumgardner, J. J. Choi, T. Hanrath, R. G. Hennig, *ACS Nano* **6**, 2118–2127 (2012).
10. P. L. McEuen, D. L. Klein, R. Roth, A. K. L. Lim, A. P. Alivisatos, *Nature* **389**, 699–701 (1997).
11. D. V. Talapin, J. S. Lee, M. V. Kovalenko, E. V. Shevchenko, *Chem. Rev.* **110**, 389–458 (2010).
12. A. H. Ip *et al.*, *Nat. Nanotechnol.* **7**, 577–582 (2012).
13. Y. W. Jun, J. H. Lee, J. S. Choi, J. Cheon, *J. Phys. Chem. B* **109**, 14795–14806 (2005).
14. S.-M. Lee, Y. W. Jun, S.-N. Cho, J. Cheon, *J. Am. Chem. Soc.* **124**, 11244–11245 (2002).
15. Materials and methods are available as supplementary materials on *Science* Online.
16. I. Moreels *et al.*, *Chem. Mater.* **19**, 6101–6106 (2007).
17. I. Moreels *et al.*, *ACS Nano* **5**, 2004–2012 (2011).
18. V. Petkov, I. Moreels, Z. Hens, Y. Ren, *Phys. Rev. B* **81**, 241304 (2010).
19. D. Britt, Y. Yoon, P. Ercius, T. D. Ewers, A. P. Alivisatos, *Chem. Mater.* **25**, 2544–2548 (2013).
20. A. J. Houtepen, R. Koole, D. Vanmaekelbergh, J. Meeldijk, S. G. Hickey, *J. Am. Chem. Soc.* **128**, 6792–6793 (2006).
21. Y. Gai, H. Peng, J. Li, *J. Phys. Chem. C* **113**, 21506–21511 (2009).
22. K. Shiraishi, *J. Phys. Soc. Jpn.* **59**, 3455–3458 (1990).
23. P. Srivastava, *Rep. Prog. Phys.* **60**, 561–613 (1997).
24. L. Manna, L. W. Wang, R. Cingolani, A. P. Alivisatos, *J. Phys. Chem. B* **109**, 6183–6192 (2005).
25. C. Fang, M. A. van Huis, D. Vanmaekelbergh, H. W. Zandbergen, *ACS Nano* **4**, 211–218 (2010).
26. K. Kimura, K. Nakajima, Y. Fujii, M. Mannami, *Surf. Sci.* **318**, 363–367 (1994).
27. G. Wulff, *Z. Krystallog.* **34**, 449 (1901).
28. E. Ringe, R. P. Van Duyne, L. D. Marks, *Nano Lett.* **11**, 3399–3403 (2011).
29. S. Polarz, *Adv. Funct. Mater.* **21**, 3214–3230 (2011).
30. P. J. Eng *et al.*, *Science* **288**, 1029–1033 (2000).
31. P. J. Feibelman, *Science* **295**, 99–102 (2002).
32. S. U. Khan, M. Al-Shahry, W. B. Ingler Jr., *Science* **297**, 2243–2245 (2002).
33. H. J. Shin *et al.*, *Nat. Mater.* **9**, 442–447 (2010).
34. W. T. Pong, C. Durkan, *J. Phys. D Appl. Phys.* **38**, R329–R355 (2005).
35. S. Wu, R. Yang, D. Shi, G. Zhang, *Nanoscale* **4**, 2005–2009 (2012).
36. X. Deng *et al.*, *Langmuir* **24**, 9474–9478 (2008).
37. K. Andersson, A. Nikitin, L. Pettersson, A. Nilsson, H. Ogasawara, *Phys. Rev. Lett.* **93**, 196101 (2004).

ACKNOWLEDGMENTS

We thank R. Cai and Z. Zhu for helpful discussions and J. Engel for help in the XPS experiments. This work was supported by the Director, Office of Science, the Office of Basic Energy Sciences, Materials Sciences and Engineering Division of the U.S. Department of Energy (DOE) through the organic/inorganic nanocomposite program under contract DE-AC02-05CH11231. It used resources of the National Energy Research Scientific Computing Center, the Molecular Foundry, and the Advanced Light Source, which are supported by the Office of Science of the DOE. Computations also used resources of the Oak Ridge Leadership Computing Facility at the Oak Ridge National Laboratory, which is supported by the Office of Science of the DOE under contract no. DE-AC05-00OR22725, with computational time allocated by the Innovative and Novel Computational Impact on Theory and Experiment project. M.S. thanks the Alexander von Humboldt-Foundation for a Feodor Lynen-Fellowship. Materials and methods, supporting information, and the coordinates of NC models are included in the supplementary materials.

SUPPLEMENTARY MATERIALS

www.sciencemag.org/content/344/6190/1380/suppl/DC1
Materials and Methods
Supplementary Text
Figs. S1 to S19
Tables S1 to S3
References (*38*–*82*)
Databases S1 and S2

27 February 2014; accepted 14 May 2014
Published online 29 May 2014;
10.1126/science.1252727

COMPUTATIONAL BIOLOGY

Controlling low rates of cell differentiation through noise and ultrahigh feedback

Robert Ahrends, Asuka Ota, Kyle M. Kovary, Takamasa Kudo, Byung Ouk Park, Mary N. Teruel*

Mammalian tissue size is maintained by slow replacement of de-differentiating and dying cells. For adipocytes, key regulators of glucose and lipid metabolism, the renewal rate is only 10% per year. We used computational modeling, quantitative mass spectrometry, and single-cell microscopy to show that cell-to-cell variability, or noise, in protein abundance acts within a network of more than six positive feedbacks to permit pre-adipocytes to differentiate at very low rates. This reconciles two fundamental opposing requirements: High cell-to-cell signal variability is needed to generate very low differentiation rates, whereas low signal variability is needed to prevent differentiated cells from de-differentiating. Higher eukaryotes can thus control low rates of near irreversible cell fate decisions through a balancing act between noise and ultrahigh feedback connectivity.

Understanding how large populations of cells direct small subsets to a different state is crucial for understanding the differentiation of precursor cells and stem cells, as well as cancer progression (*1*). Adipocyte differentiation is of fundamental importance for disease-associated conditions such as insulin resistance, obesity, and cancer and is also an accessible experimental system for investigating mammalian cell fate decisions. Adipocytes have a large pool of precursor cells that reside in the fat tissue—about one for every five differentiated cells (*2*)—which means that only about 1 cell out of 60 embarks on a differentiation path during the up to 12 days it takes to differentiate (*3*) (supplementary text). These pre-adipocytes differentiate through a bistable switch mechanism with a single threshold for activation in each cell that involves positive feedback between two key transcription factors, CCAAT/enhancer binding protein α (CEBPA) and peroxisome proliferator-activated receptor γ (PPARG) (Fig. 1A) (*4*). In a bistable system, if the precursor population were truly uniform, there would be a single critical threshold stimulus below which 100% of the cells remain precursor cells and above which 100% of the cells differentiate. Thus, it is a conundrum how a graded response is observed experimentally (Fig. 1B) (*5*), with weak stimuli inducing very low differentiation rates that increase as the stimuli intensity increases rather than causing all cells to convert at one critical stimulus threshold.

By extension of results from bacterial differentiation (*6*), it is plausible that the observed regulated mammalian differentiation rates are generated by noise, or cell-to-cell variability, in the abundance of key regulatory proteins (*7*–*10*).

Department of Chemical and Systems Biology, Stanford University, Stanford, CA 94305, USA.
***Corresponding author. E-mail: mteruel@stanford.edu**

Science

Hydroxylation of the surface of PbS nanocrystals passivated with oleic acid

Danylo Zherebetskyy, Marcus Scheele, Yingjie Zhang, Noah Bronstein, Christopher Thompson, David Britt, Miquel Salmeron, Paul Alivisatos and Lin-Wang Wang

Science **344** (6190), 1380-1384.
DOI: 10.1126/science.1252727originally published online May 29, 2014

Nanoparticle lattices and surfaces

The challenge of resolving the details of the surfaces or assemblies of colloidal semiconductor nanoparticles can be overcome if several characterization methods are used (see the Perspective by Boles and Talapin). Boneschanscher *et al.* examined honeycomb superlattices of lead selenide nanocrystals formed by the bonding of crystal faces using several methods, including high-resolution electron microscopy and tomography. The structure had octahedral symmetry with the nanocrystals distorted through "necking": the expansion of the contact points between the nanocrystals. Zherebetskyy *et al.* used a combination of theoretical calculations and spectroscopic methods to study the surface layer of lead sulfide nanocrystals synthesized in water. In addition to the oleic acid groups that capped the nanocrystals, hydroxyl groups were present as well.

Science, this issue p. 1377, p. 1380; see also p. 1340